Solid State Communications 370 (2023) 115235

Contents lists available at ScienceDirect

Solid State Communications

journal homepage: www.elsevier.com/locate/ssc

Cubic-phase $NaYF_4:Pr^{3+}$, Yb^{3+} down-conversion phosphors for optical temperature sensing

M.S. Pudovkin [a,*], S.V. Kuznetsov [a,b], V.A. Konuyshkin [b], A.N. Nakladov [b], V.V. Voronov [b]

[a] Kazan Federal University, Institute of physics, 18 Kremlyovskaya Str, Kazan, 420008, Russian Federation
[b] Prokhorov General Physics Institute of the Russian Academy of Sciences, 38 Vavilov Str., Moscow, 119991, Russian Federation

ARTICLE INFO

Communicated by: Zhao Liuyan

Keywords:
Cubic-phase $NaYF_4:Pr^{3+}$
Yb^{3+}
Down-conversion
Luminescent thermometry
Optical temperature sensors

ABSTRACT

The cubic phase $NaYF_4:Pr^{3+}$, Yb^{3+} single crystals were grown in the resistive furnace by the Bridgman-Stockbarger technique with following milling in an agate mortar. The luminescence intensity ratio (LIR) between $^3P_1 - {}^3H_5$ and $^3P_0 - {}^3H_5$ emissions of Pr^{3+} was taken a temperature-dependent parameter. The calculated absolute (S_a) temperature sensitivity was 0.0075 at 320 K. The LIR between $^3P_0 - {}^1G_4$ (Pr^{3+}) and $^2F_{5/2} - {}^2F_{7/2}$ (Yb^{3+}) emissions is also temperature-dependent due to phonon-assisted nature of energy transfer between $^1G_4$ of Pr^{3+} and $^2F_{5/2}$ of Yb^{3+}. S_r and S_a demonstrated the highest values in the 100–220 K temperature range (S_a (max) = 0.0047 K^{-1} at 150 K).

$NaYF_4:Pr^{3+}$, Yb^{3+} samples are useful in optical temperature sensing in the broad temperature range from 100 up to 320 K.

1. Introduction

Rare-earth doped fluoride matrixes are very promising luminescence materials due to the sharp emission bands, lack of photobleaching, high chemical stability [1–4], and low cytotoxicity [5]. Among a huge variety of fluoride materials, double-doped materials hold a special role [6,7]. In this case, one ion serves as a donor of excitation energy the second one serves as an acceptor. Such luminophores are multifunctional and able to convert higher energy irradiation (ultraviolet and/or visible light) into lower energy irradiation (generally near-infrared light) [8,9]. This property is highly demanded in the solar cell industry [6,7,10]. Specifically, crystalline nano- and microparticles doped with Pr^{3+}/Yb^{3+} ion pair are capable of converting blue light (~440–470 nm spectral range, $^3P_J - {}^3H_4$ transitions of Pr^{3+} ions (J = 0, 1, 2)) into near-infrared light (~950–1050 nm range, $^2F_{5/2} - {}^2F_{7/2}$ transition of Yb^{3+} ions). In turn, crystalline nano- and microparticles doped with Nd^{3+}/Yb^{3+} ion pair are capable of converting both ultraviolet and visible light (350–460 nm spectral range, ^4D_J, $^2P_{3/2}$, $^4G_J - {}^4I_{9/2}$ transitions of Nd^{3+}) into near-infrared light (~950–1050 nm, $^2F_{5/2} - {}^2F_{7/2}$ transition of Yb^{3+}) [6,11]. The down-conversion occurs via two main mechanisms: quantum cutting and phonon-assisted energy transfer between particular electron levels. The phonon-assisted energy transfer between Pr^{3+} and Yb^{3+} ions occurs between $^2F_{5/2}$ of Yb^{3+} and $^1G_4$ of Pr^{3+}.

The efficiency of phonon-assisted energy transfer is temperature-dependent which paves the way toward optical temperature sensing based on a luminescence signal of down-conversion phosphors. Indeed, the luminescence intensity of acceptor ion depends on the efficiency of phonon-assisted energy transfer from donor ion. Hence, the spectrum shape is temperature-dependent. In this case, the luminescence intensity ratio (LIR) of donor and acceptor emissions can be taken as a temperature-dependent parameter [12].

In luminescence thermometry, a great attention should be paid to the calibration of the system. It means that the temperature dependence of the chosen luminescence parameter should be studied as carefully as possible. There are some hidden pitfalls that should be taken into consideration. Indeed, for such hosts as $LiREF_4$ (RE = Y, Gd etc.) and Li(Y,Lu)F_4 the bulk crystals have anisotropy of the luminescence properties due to the tetragonal crystal structure [13]. Simply, it means that the luminescence spectrum shape depends on the direction of the observation. The calibration of the phosphors is usually performed for nano-powders, micropowders or the crystals with known axes directions. The nano- or microparticles have different angles of the axes in reference to the detector. Hence, the luminescence signal is averaged. However, if the temperature reading is carried out from a single particle that is in contact with the studied object, the position of the crystal axis is usually unknown. Hence, the calibration data of the powder cannot be applied

* Corresponding author. Department of quantum electronics and radiospectroscopy, Kazan Federal University, 18 Kremljovskaya str., Kazan, 420008, Russia.
E-mail address: jaz7778@list.ru (M.S. Pudovkin).

https://doi.org/10.1016/j.ssc.2023.115235
Received 20 July 2022; Received in revised form 22 December 2022; Accepted 30 May 2023
Available online 1 June 2023

to a single particle. The cubic-phase materials do not demonstrate such peculiarities, hence the calibration can be performed for a powder but the obtained dependence can be applied for a single particle. It makes the cubic-phase-based materials more universal. In order to meet these requirements, we have chosen a cubic-phase $NaYF_4$ host. This host has also low phonon energy (~350 cm^{-1}) [14], high transparency, and high chemical stability [15].

Early, we clearly demonstrated that the Pr^{3+}/Yb^{3+} down-conversion ionic pair is very promising for optical temperature sensing [16]. Indeed, the ratio between Pr^{3+} and Yb^{3+} emissions is temperature dependent due to phonon-assisted nature of excitation energy exchange between these ions. These experiments were performed for one composition of Pr^{3+} (0.1 mol.%) and Yb^{3+} (10.0 mol.%) in the $Ba_4Y_3F_{17}$ host because very low luminescence signal was observed for other concentrations. Moreover, it is still an intricate task to choose proper concentrations of both Pr^{3+} and Yb^{3+} in order to achieve intense luminescence of both Pr^{3+} and Yb^{3+} ions [16].

The paper is devoted to the study the influence of doping ion concentration on the temperature sensitivity of the cubic-phase $NaYF_4:Pr^{3+}$, Yb^{3+} phosphors. In order to avoid the undesirable luminescence quenching as well as to enlarge signal-to-noise ratio, we used microparticles prepared from the bulk crystals by mechanical milling. The choice of Pr^{3+} and Yb^{3+} concentrations was based on the requirement of obtaining the intense luminescence signal of both Pr^{3+} and Yb^{3+} ions.

In our opinion, the main novelty of this research is that the thermometric characteristics of double-doped Pr^{3+}/Yb^{3+} inorganic phosphors are significantly less studied compared to single-doped Pr^{3+} ones.

2. Materials and methods

2.1. 1Crystal growth and sample preparation

The samples were synthesized by high-temperature melting of initial fluoride components in a vacuum with CF_4 fluorinating atmosphere for preventing of the pyrohydrolysis. The crystal growth procedure was based on the analysis of the phase diagram of NaF-YF_3 [17]. The region of primary crystallization of the cubic modification does not correspond to 50 mol.% (NaF):50 mol.% (YF_3). A set of solid solutions with general formula $Na_{0.4}Y_{0.6-x-y}Yb_xPr_yF_{2.2}$ was synthesized. Sodium fluoride (chemically pure, LANHIT, Russia), yttrium fluoride (purity grade 99.99, LANHIT, Russia), ytterbium fluoride (purity grade 99.99, LANHIT, Russia), praseodymium fluoride (purity grade 99.99, LANHIT, Russia) were used as starting chemicals. The initial components of the mixture were carefully ground in a jasper mortar with pestle and transferred to graphite crucible. The crucible was placed in a vacuum furnace and evacuated up to vacuum of 10^{-3} mm Hg with gradually heating up to 1000 °C. After these procedure, the fluorinating agent (CF_4) was injected to a residual pressure of 0.9 atm. Crucible was pulled from the hot zone to the cold zone at a rate of 10 mm/h and cooled to room temperature. As a result, the concentration series of $Na_{0.4}Y_{0.6-x-y}Yb_xPr_yF_{2.2}$ solid solutions were prepared. The resulting samples were carefully ground in a jasper mortar for 20 min in order to obtain a homogeneous powder.

2.2. Material characterization

The luminescence spectra were detected using the CCD spectrometer (StellarNet) with 0.5 nm spectral resolution. The CW diode laser was used for luminescence excitation at $\lambda_{ex} = 442$ nm, which corresponds to most intensive absorption band of Pr^{3+} ion ($^3H_4 - {}^3P_2$) [18]. The experiments were carried out in 80–320 K temperature range. The temperature control was carried out by "CRYO industries" thermostatic cooler with LakeShore Model 325 temperature controller (USA). The liquid nitrogen was used as a cooling agent. The power density of excitation irradiation was measured using a PULSAR-2 powermeter (Ophir laser measurement group) with StarLab (pulsar sensor 2) software.

The registration of temperature-dependent parameters was carried out in thermally stable conditions without heating from excitation irradiation. The shape of the Pr^{3+} spectrum in fluoride hosts especially in the 520–550 nm range with two $^3P_0 - {}^3H_4$ and $^3P_1 - {}^3H_4$ transitions is temperature-dependent due to thermally-coupled nature of $^3P_1$ and $^3P_0$ levels in 200–600 K range [19]. In our experiments the spectrum shape does not change during the excitation procedure because the heating did not occur or can be neglected at the chosen excitation power density (1350 W/m^2). Two sets of samples such as $NaYF_4:Pr^{3+}$ (0.1 mol.%), Yb^{3+} (0.5; 1.0; and 5.0 mol.%) and $NaYF_4:Pr^{3+}$(0.05; 1.0 mol.%), Yb^{3+}(0.5 mol.%) were analyzed.

3. Results and discussion

3.1. Room temperature spectral characterization of $NaYF_4:Pr^{3+}$, Yb^{3+}

An energy level diagram and the normalized (at 601 nm peak) room temperature luminescence spectra of both $NaYF_4:Pr^{3+}$(0.1 mol.%), Yb^{3+} (0.5; and 1.0 mol. %) samples are represented in Fig. 1 a and **b,** respectively.

The observed intense emission of Yb^{3+} ions under the excitation of Pr^{3+} ones demonstrates an energy transfer from Pr^{3+} to Yb^{3+}. All the emission peaks were interpreted as result of transitions from $^3P_1$ and $^3P_0$ levels of Pr^{3+} to the lower energy levels [20–22]. The Yb^{3+} peak ($^2F_{5/2} - {}^2F_{7/2}$, ~950–1050 nm range) was also identified. Unidentified transitions were not observed. Interestingly, that the samples demonstrate intense $^3P_{1,0} - {}^1G_4$ peaks in the ~850–950 nm range. The same tendency was observed in $LaF_3:Pr^{3+}$, Yb^{3+} samples [23]. The $^3P_{1,0} - {}^1G_4$ emission is notably weaker in comparison to another Pr^{3+}/Yb^{3+} doped matrices such as YOF, CaF_2, $Ba_4Y_3F_{17}$ [9,10,16].

There are three mechanisms providing the population of $^2F_{5/2}$ level of Yb^{3+} under the excitation of Pr^{3+} ions. The first one is quantum cutting because one high energy "blue" photon is "cut" into two photons having smaller energy [11,22,24]. The second one is a phonon-assisted energy transfer from $^1G_4$ of Pr^{3+} to $^2F_{5/2}$ of Yb^{3+}. The third mechanism is the cross-relaxation between Pr^{3+} ($^3P_0 - {}^1G_4$) and Yb^{3+} ($^2F_{7/2} - {}^2F_{5/2}$) [18]. However, the cross-relaxation was observed for 3% Yb^{3+} concentration and higher ones. It can be suggested that both quantum mechanisms (quantum cutting and cross-relaxation) demonstrate weak temperature dependence. Thus, the temperature dependence of spectral characteristics of the studied Pr^{3+}/Yb^{3+} system is based on phonon-assisted processes including phonon-assisted energy transfer from $^1G_4$ of Pr^{3+} to $^2F_{5/2}$ of Yb^{3+}.

3.2. Temperature-depended spectral characterization of $NaYF_4:Pr^{3+}$, Yb^{3+}

The temperature evolution of the $NaYF_4:Pr^{3+}$ (0.1 mol. %), Yb^{3+} (1.0 mol %) luminescence spectra normalized at 601 nm peak in the 80–320 K temperature range is represented in Fig. 2.

The spectral shape is notably dependent on temperature in the studied 80–320 K range. The intensity of $^3P_1 - {}^3H_J$ (J = 3, 4, and 5) emissions increases with the increase of temperature. This phenomenon is related to the well-known fact that $^3P_1$ and $^3P_0$ levels of Pr^{3+} ions are thermally coupled [25]. These levels share their electron populations according to the Boltzmann law. The $NaYF_4:Pr^{3+}$ (0.1 mol.%), Yb^{3+} (1.0 mol. %) luminescence spectra detected in the 80–320 K range ($^3P_1 - {}^3H_5$ and $^3P_0 - {}^3H_5$ emission peaks) are represented in Fig. 3.

LIR between $^3P_1 - {}^3H_5$ and $^3P_0 - {}^3H_5$ emission peaks was taken as a temperature-dependent parameter (Fig. 4). Since the $^3P_1$ and $^3P_0$ levels of Pr^{3+} ions share their electron populations according to the Boltzmann law, the LIR was fitted by the exponential function according to the Boltzmann law [25]:

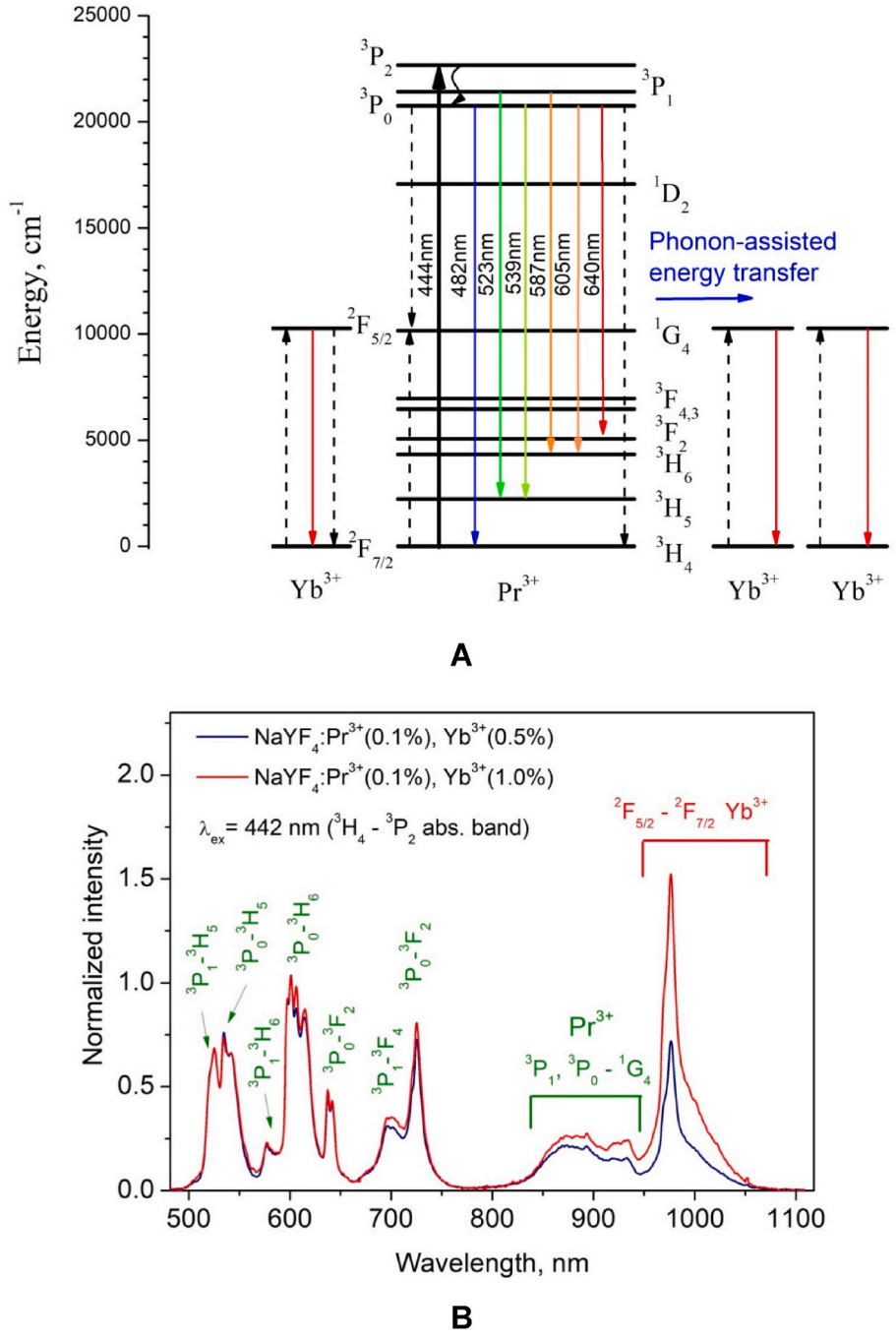

Fig. 1. a. Energy level diagram of $NaYF_4:Pr^{3+}$, Yb^{3+}, b. Normalized (at 601 nm peak) room temperature luminescence spectra of $NaYF_4:Pr^{3+}$ (0.1 mol.%), Yb^{3+} (0.5; and 1.0 mol. %) samples. Excitation wavelength 442 nm corresponds to the $^3H_4$ – $^3P_2$ absorption band of Pr^{3+} ion.

$$LIR = Bexp\left(-\frac{\Delta E}{k_B T}\right) + C \tag{1}$$

where B and C are constants; k_B is the Boltzmann constant, T is absolute temperature; ΔE is the activation energy. In the case of phosphors based on the Boltzmann law, the ΔE is an effective energy difference between two thermally coupled levels. The absolute temperature T was expressed by equation (2):

$$T = \frac{\Delta E}{k_B \, Ln\left(\frac{B}{LIR}\right)} \tag{2}$$

The obtained $\Delta E = 729 \pm 14$ cm^{-1} value is slightly larger than the theoretical values [25,26]. This fact was explained by the overlap between $^3P_1$– $^3H_5$ and $^3P_0$ – $^3H_5$ emission peaks, which is very common for Boltzmann-based optical sensors.

For temperature sensing applications, the absolute temperature sensitivity S_a and relative temperature sensitivity S_r are very important characteristics. The S_a [parameter units/K] and S_r [%/K] are determined as:

$$S_a = \left|\frac{d(LIR)}{dT}\right| \tag{3}$$

$$S_r = \frac{1}{LIR}\left|\frac{d(LIR)}{dT}\right| \bullet 100\% \tag{4}$$

The S_a and S_r curves for 80–320 K temperature range are represented

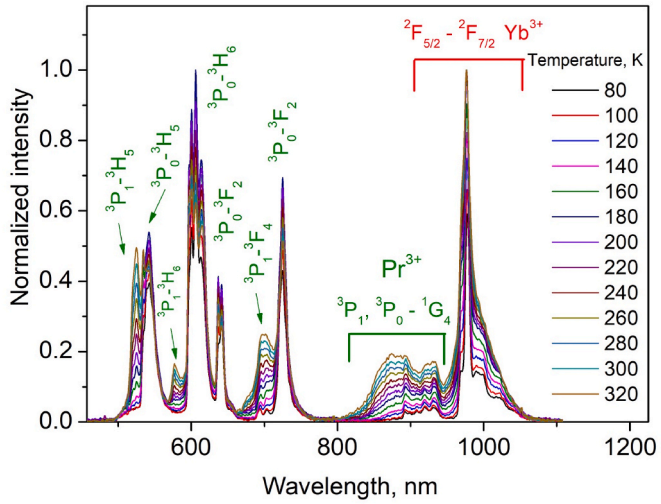

Fig. 2. Temperature evolution of the $NaYF_4$:Pr^{3+} (0.1 mol.%), Yb^{3+} (1.0 mol. %) normalized at 601 nm luminescence spectra in the 80–320 K temperature range.

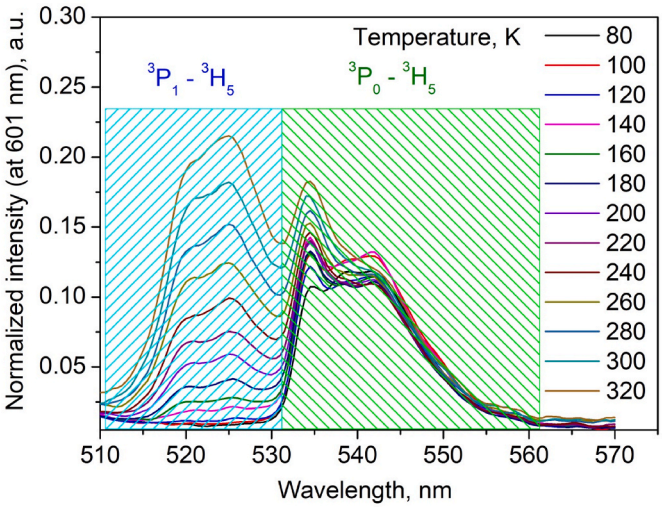

Fig. 3. Temperature evolution of the $NaYF_4$:Pr^{3+} (0.1 mol.%), Yb^{3+} (1.0 mol. %) normalized at 601 nm luminescence spectra in the 80–320 K temperature range (500–570 nm spectral range).

in Fig. 4b.

The LIR between $^3P_1$,$^3P_0$ – $^1G_4$ emission (~800–960 nm) of Pr^{3+} and $^2F_{5/2}$ – $^2F_{7/2}$ emission of Yb^{3+} (~960–1050 nm) was chosen as a temperature-dependent parameter. There is a phonon-assisted energy transfer between $^1G_4$ of Pr^{3+} and $^2F_{5/2}$ of Yb^{3+} and efficiency of $^2F_{5/2}$ population depends on the efficiency of $^1G_4$ population. The LIR based on $^1G_4$ – ^3H_j emission of Pr^{3+} is also useful but these emissions are in the 1300–1400 nm range [23]. It is more difficult to detect these emissions due to lower energy of "infrared" photons. The LIR between $^3P_1$,$^3P_0$ – $^1G_4$ emission (~800–960 nm) of Pr^{3+} and $^2F_{5/2}$ – $^2F_{7/2}$ emission of Yb^{3+} (~960–1050 nm) is represented in Fig. 5.

LIR curves of the samples grow gradually in the 120–320 K temperature range. In the 80–120 K range, LIR temperature dependence is negligible. It can be related to the low probability of phonon appearance at such low temperatures. The growth rate of the LIR functions does not differ significantly between each other. The growing character of the curves is attributed to the Yb^{3+} intensity growth with the temperature increase. The quantum cutting process and cross-relaxation are not phonon-assisted processes. Suggestively, these processes have low

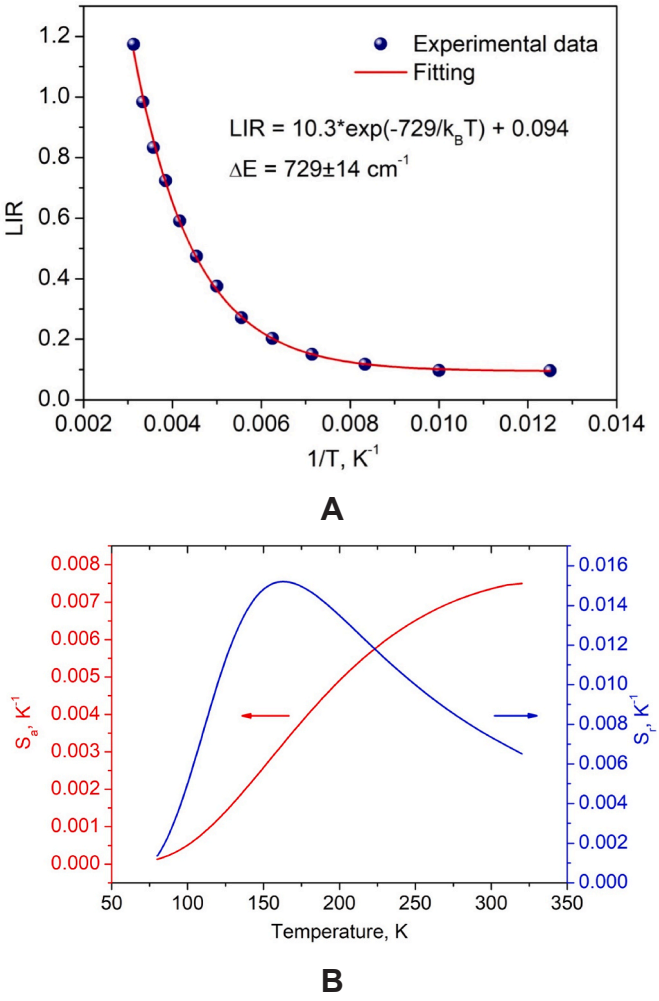

Fig. 4. a. Luminescence integrated intensity ratio (LIR) of $^3P_1$ – $^3H_5$ and $^3P_0$ – $^3H_5$ emission peaks as a function of inverse temperature. The fitting curve is an exponential decay function

Fig.4 b. Absolute (S_a) and relative (S_r) temperature sensitivities as functions of temperature for $NaYF_4$:Pr^{3+} (0.1 mol.%), Yb^{3+} (1.0 mol %) sample.

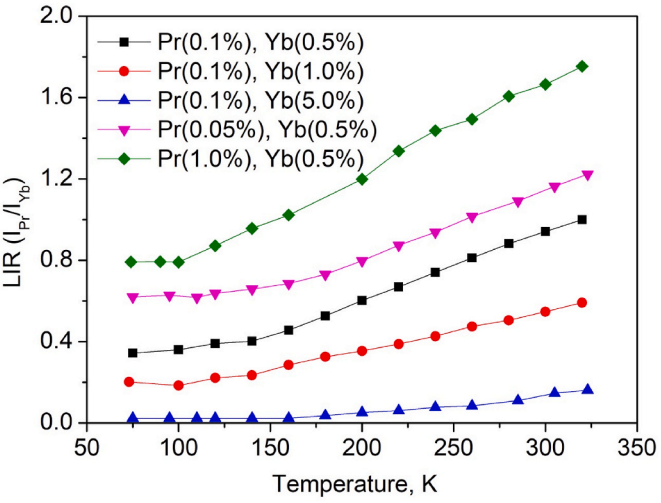

Fig. 5. Luminescence intensity ratio (LIR) between $^3P_1$,$^3P_0$ – $^1G_4$ emission (~800–960 nm) of Pr^{3+} and $^2F_{5/2}$ – $^2F_{7/2}$ emission of Yb^{3+} (~960–1050 nm). The lines serve as eye-trackers.

sensitivity to temperature in comparison to phonon-assisted processes. The slight difference in the slopes of the LIR curves was explained by the phonon-assisted back energy transfer from Yb^{3+} to Pr^{3+}. Also, the different grade of overlapping of $^3P_{0,1}$ – $^1G_4$ (Pr^{3+}) and $^2F_{5/2}$ – $^2F_{7/2}$ (Yb^{3+}) emissions can contribute to the slight difference in growth rate of LIR curves.

Since, there is no significant difference in the LIR behavior, $NaYF_4$:Pr^{3+} (0.1 mol.%), Yb^{3+} (0.5 mol.%) sample was chosen for further research. This sample demonstrates the highest signal-to-noise ratio supposedly due to the lowest concentrations of the doping ions. Unfortunately, the above-mentioned LIR curves do not demonstrate notable temperature sensitivities. The most effective LIR parameter is based on two emissions, which demonstrate opposite temperature behaviors. For example, one emission increases while another one decreases with the temperature change. In this case, the electron population of $^3P_0$ decreases by populating the $^3P_1$ level with the temperature increase. Hence, the $^3P_0$ – $^1G_4$ or $^3P_0$ – ^3H_J (J = 4, 5, and 6) emissions decrease with the increase of temperature. On the other hand, the Yb^{3+} emission increases with the temperature increase. According to Ref. [16] for Pr^{3+}/Yb^{3+} pair, the LIR between $^3P_0$ – $^3H_5$ and $^2F_{5/2}$ – $^2F_{7/2}$ emissions has temperature-dependent correlation. This LIR as a temperature function is represented in Fig. 6. Since Equation (1) is not appropriate for non-thermally coupled energy levels, the experimental LIR was well fitted by a polynomial function as it was done in Refs. [27,28]. The 4th order polynomial provides the best fitting ($R^2 = 0.998$).

This LIR depends on temperature in the whole temperature range in comparison to the LIR calculated for $^3P_1$,$^3P_0$ – $^1G_4$ (Pr^{3+}) and $^2F_{5/2}$ – $^2F_{7/2}$ (Yb^{3+}) emissions. S_a and S_r curves are represented in Fig. 7.

Both sensitivities demonstrate the highest values in the 120–220 K temperature range (maximum $S_a = 0.0047\ K^{-1}$ at 150 K). These values are larger in comparison to $LiLaP_4O_{12}$:Nd^{3+},Yb^{3+} (maximum $S_a = 0.0020\ K^{-1}$ at 150 K) [29] and YF_3:Nd^{3+},Yb^{3+} (maximum $S_a = 0.0015$ at 150 K) [11]. Values of S_a and S_r in comparison to another matrixes of the studied samples are summarized in Table 1 Note, that for some phosphors S_a values are not presented in the papers.

The achieved characteristics are quite competitive compared to the world analogs. However, the majority of sensitivity values from the cited papers were calculated for non-cubic phase substances with anisotropy of luminescence properties. This feature does not allow temperature reading from a single particle. The cubic Tb^{3+}, Eu^{3+}:CaF_2 has almost the same characteristics as the studied sample. However, in the CaF_2 host, the Ca^{2+} can lead to partial reduction of Yb oxidation state from 3+ up to 2+ with changing of spectral properties. Thus, the additional attention to the synthesis procedure and the control of valence should be paid. In these terms, the cubic $NaYF_4$ (with Y^{3+}) host seems to be more preferable because the partial reduction of Yb oxidation state does not occur.

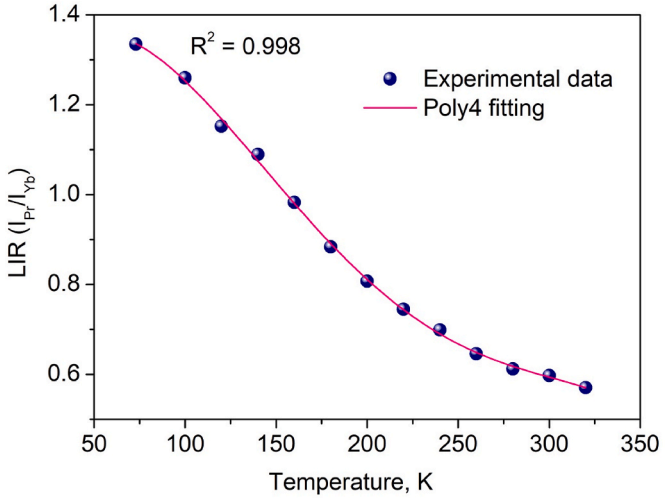

Fig. 6. LIR between $^3P_0$ – $^3H_5$ and $^2F_{5/2}$ – $^2F_{7/2}$ emissions as a function of temperature. The experimental data were fitted by 4th order polynomial function ($LIR(T) = 1.15 + 0.009\ T – 1.14\ T^2 + 3.94\ T^3 – 4.42\ T^4$).

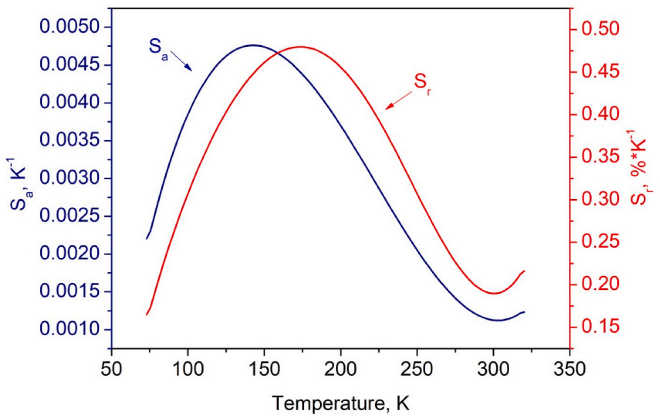

Fig. 7. Absolute (S_a, [K^{-1}]) and relative (S_r, [%*K^{-1}]) temperature sensitivities as functions of temperature for $NaYF_4$:Pr^{3+} (0.1 mol.%), Yb^{3+} (0.5 mol. %) sample.

4. Conclusions

The luminescence intensity ratio (LIR) between $^3P_1$ – $^3H_5$ and $^3P_0$ – $^3H_5$ emission peaks was taken as a temperature-dependent parameter. The calculated absolute (S_a) temperature sensitivity was 0.008 K^{-1} at 320 K. The LIR between $^3P_0$ – $^1G_4$ (Pr^{3+}) and $^2F_{5/2}$ – $^2F_{7/2}$ (Yb^{3+}) emission peaks is also temperature-dependent. This phenomenon was explained by phonon-assisted nature of energy transfer between $^1G_4$ of Pr^{3+} and $^2F_{5/2}$ of Yb^{3+}. S_r and S_a demonstrated the highest values in the 100–220 K temperature range (maximum $S_a = 0.0047\ K^{-1}$ at 150 K), which are quite competitive compared to the world analogs. However, the majority of the inorganic competitors do not have cubic phase, hence, the anisotropy of luminescence properties can take place. In turn, the cubic phase of the particles allows temperature reading from a single particle that is in contact with the studied object. Finally the $NaYF_4$:Pr^{3+}, Yb^{3+} samples can be applied as optical temperature sensors in the broad temperature range (~100–320 K). In the 100–220 K the LIR between $^3P_0$ – $^1G_4$ (Pr^{3+}) and $^2F_{5/2}$ – $^2F_{7/2}$ (Yb^{3+}) emission peaks is used. In the 220–320 K range, the use of LIR between $^3P_1$ – $^3H_5$ and $^3P_0$ – $^3H_5$ emission peaks of Pr^{3+} is more efficient. The cubic phase of the particles allows temperature reading from a single particle.

Credit author statement

We the undersigned declare that this manuscript is original, has not been published before and is not currently being considered for publication elsewhere. We confirm that the manuscript has been read and approved by all named authors and that there are no other persons who satisfied the criteria for authorship but are not listed. We further confirm that the order of authors listed in the manuscript has been approved by all of us. We understand that the Corresponding Author is the sole contact for the Editorial process. He/she is responsible for communicating with the other authors about progress, submissions of revisions and final approval of proofs Signed by all authors as follows.

Declaration of competing interest

The authors declare that they have no known competing financial interests or personal relationships that could have appeared to influence the work reported in this paper.

Table 1
The comparison of luminescence thermometer performances of double-doped rare-earth down-conversion phosphors in the 100–220 K temperature range. LIR is taken as a temperature-dependent parameter.

Sample and phase	Transitions and wavelengths for LIR (I_1/I_2) and optical excitation conditions	Maximum S_a [K^{-1}] in the 100–220 K range	Maximum S_r [$\%K^{-1}$] in the 100–220 K range	Ref.
Pr^{3+},Yb^{3+}:$NaYF_4$ (cubic)	I_{Pr} ($^3P_0$ – $^1G_4$, ~810–966 nm)/I_{Yb} ($^2F_{5/2}$ – $^2F_{7/2}$, ~980 nm), λ_{ex} = 442 nm, CW laser, $^3H_4$ – $^3P_2$ absorption band of Pr^{3+} ion	$4.7{\cdot}10^{-3}$	0.45	This work
Nd^{3+}(0.5%),Yb^{3+}(1.0%):YF_3 (orthorhombic)	I_{Nd} ($^4F_{3/2}$ – $^4I_{9/2}$, ~866 nm)/I_{Yb} ($^2F_{5/2}$ – $^2F_{7/2}$, ~980 nm), λ_{ex} = 355 nm, pulse laser	$1.8{\cdot}10^{-3}$	0.58 (at 145 K)	[11]
Nd^{3+}(1%),Yb^{3+}(0.5–5%): $LiLaP_4O_{12}$ (monoclinic)	I_{Nd} ($^4F_{3/2}$ – $^4I_{9/2}$, ~866 nm)/I_{Yb} ($^2F_{5/2}$ – $^2F_{7/2}$, ~980 nm), λ_{ex} = 808 nm, CW laser	–	From 0.05 to 0.25 (depends on the Yb^{3+} concentration)	[29]
Tb^{3+}, Eu^{3+}:CaF_2 (cubic)	I_{Tb} ($^5D_4$ – $^7F_5$, ~545 nm)/I_{Eu} ($^5D_0$ – $^7F_2$, ~615 nm), λ_{ex} = 485 nm pulse laser	$4.0{\cdot}10^{-3}$	–	[30]
Pr^{3+}(0.1%),Yb^{3+}(10.0%): $Ba_4Y_3F_{17}$ (hexagonal)	I_{Pr} ($^4F_{3/2}$ – $^4I_{9/2}$)/I_{Yb} ($^2F_{5/2}$ – $^2F_{7/2}$), λ_{ex} = 442 nm, pulse laser	$1.0{\cdot}10^{-3}$	0.20	[16]
Tb^{3+}(6.0%),Eu^{3+}(8.0%): $Ca_5(PO_4)_3F$ (hexagonal)	I_{Tb} ($^5D_4$ – $^7F_5$, ~548 nm)/I_{Eu} ($^5D_0$ – $^7F_2$, ~621 nm), λ_{ex} = 299 nm, laser	$1.31{\cdot}10^{-3}$	0.40	[31]
MoO_3:Eu^{3+}, Tb^{3+} (cubic)	I_{Tb} ($^5D_4$ – $^7F_5$, ~548 nm)/I_{Eu} ($^5D_0$ – $^7F_2$, ~621 nm)	~10^{-3} at 105 K, not studied at higher temperatures	~0.50 at 105 K, not studied at higher temperatures	[32]
Yb^{3+},Tm^{3+}:$NaGdTiO_4$ (orthorhombic)	I_{Tm} ($^3H_4$ (1) →$^3H_6$, 812 nm)/I_{Tm} ($^3H_4$ (2) →$^3H_6$, 798 nm), λ_{ex} = 980 nm, CW laser	$2.0{\cdot}10^{-3}$ at 100 K and $1.0{\cdot}10^{-3}$ at 200 K	–	[33]
Pr^{3+}:LaF_3 (hexagonal)	I_{Pr} ($^3P_1$→$^3H_5$, 523 nm)/I_{Pr} ($^3P_0$→$^3H_5$, 537 nm), λ_{ex} = 442 nm, pulse laser	$0.5{\cdot}10^{-3}$ at 100 K	–	[34]
LaF_3:Pr^{3+},Yb^{3+} (hexagonal)	I_{Pr} ($^1G_4$ – $^3H_4$, ~1300–1400 nm)/I_{Yb} ($^2F_{5/2}$ – $^2F_{7/2}$, ~980 nm), λ_{ex} = 442 nm, CW laser, $^3H_4$ – $^3P_2$ absorption band of Pr^{3+} ion	0.5 at 20 K (not studied above 110 K)	–	[23]
LaF_3:Er^{3+},Yb^{3+} (hexagonal)	$^4I_{13/2}$ – $^4I_{15/2}$ (Er^{3+} ~1539.8 nm)/I_{Yb} ($^2F_{5/2}$ – $^2F_{7/2}$, ~980 nm), λ_{ex} = 378 nm, laser,	5.7 $0.5{\cdot}10^{-3}$ at 20 K (not studied above 110 K)		[23]

Data availability

Data will be made available on request.

Acknowledgments

The study was funded by the grant from the Russian Science Foundation number 22-72-00129.

References

[1] C. Liu, Y. Hou, M. Gao, Are rare-earth nanoparticles suitable for in vivo applications? Adv. Mater. 26 (40) (2014) 6922–6932, https://doi.org/10.1002/adma.201305535.
[2] X. Wang, Y. Li, Fullerene-like rare-earth nanoparticles, Angew. Chem. Int. Ed. 42 (30) (2003) 3497–3500, https://doi.org/10.1002/anie.200351006.
[3] R. Naccache, Q. Yu, J.A. Capobianco, The fluoride host: nucleation, growth, and upconversion of lanthanide-doped nanoparticles, Adv. Opt. Mater. 3 (4) (2015) 482–509, https://doi.org/10.1002/adom.201400628.
[4] V.V. Semashko, S.L. Korableva, P.P. Fedorov, Lithium rare-earth fluorides as photonic materials: 2. Some physical, spectroscopic, and lasing characteristics, Inorg. Mater. 58 (5) (2022) 447–492, https://doi.org/10.31857/S0002337X22050025.
[5] M.S. Pudovkin, P.V. Zelenikhin, A.O. Krasheninnikova, S.L. Korableva, A. S. Nizamutdinov, E.M. Alakshin, M.K. Kadirov, Photoinduced toxicity of PrF3 and LaF3 nanoparticles, Opt Spectrosc. 121 (4) (2016) 538–543, https://doi.org/10.1134/S0030400X16100209.
[6] L. Aarts, B.V.D. Ende, M.F. Reid, A. Meijerink, Downconversion for solar cells in YF3: Pr3+, Yb3+, Spectrosc. Lett. 43 (5) (2010) 373–381.
[7] D. Chen, Y. Yu, H. Lin, P. Huang, Z. Shan, Y. Wang, Ultraviolet-blue to near-infrared downconversion of Nd 3+-Yb 3+ couple, Opt. Lett. 35 (2) (2010) 220–222.
[8] W. Romero-Romo, S. Carmona-Téllez, R. Lozada-Morales, O. Soriano-Romero, U. Caldiño, M.E. Álvarez-Ramos, A.N. Meza-Rocha, Down-shifting and down-conversion emission properties of novel CdO–P2O5 invert glasses activated with Pr3+ and Pr3+/Yb3+ for photonic applications, Opt. Mater. 116 (2021), 111009, https://doi.org/10.1016/j.optmat.2021.111009.
[9] N.A.M. Saeed, E. Coetsee, H.C. Swart, Down-conversion of YOF: Pr3+, Yb3+ phosphor, Opt. Mater. 110 (2020), 110516, https://doi.org/10.1016/j.optmat.2020.110516.
[10] S.V. Kuznetsov, O.A. Morozov, V.G. Gorieva, M.N. Mayakova, M.A. Marisov, V. V. Voronov, P.P. Fedorov, Synthesis and luminescence studies of CaF2: Yb: Pr solid solutions powders for photonics, J. Fluor. Chem. 211 (2018) 70–75, https://doi.org/10.1016/j.jfluchem.2018.04.008.
[11] M.S. Pudovkin, A.K. Ginkel, E.V. Lukinova, Temperature sensitivity of Nd3+, Yb3+: YF3 ratiometric luminescent thermometers at different Yb3+ concentration, Opt. Mater. 119 (2021), 111328, https://doi.org/10.1016/j.optmat.2021.111328.
[12] P. Villanueva-Delgado, K.W. Kramer, R. Valiente, Simulating energy transfer and upconversion in β-NaYF4: Yb3+, Tm3+, J. Phys. Chem. C 119 (41) (2015) 23648–23657, https://doi.org/10.1021/acs.jpcc.5b06770.
[13] V.G. Gorieva, A.A. Lyapin, S.L. Korableva, P.A. Ryabochkina, V.V. Semashko, Spatial anomalies in spectral-kinetic properties of Pr3+-Doped LiY1-xLuxF4 mixed crystals, J. Lumin. 222 (2020), 117172, https://doi.org/10.1016/j.jlumin.2020.117172.
[14] D. Kumar, S.K. Sharma, S. Verma, V. Sharma, V. Kumar, A short review on rare earth doped NaYF4 upconverted nanomaterials for solar cell applications, Mater. Today: Proc. 21 (2020) 1868–1874, https://doi.org/10.1016/j.matpr.2020.01.243.
[15] P.P. Fedorov, A.A. Luginina, S.V. Kuznetsov, V.V. Osiko, Nanofluorides, J. Fluor. Chem. 132 (12) (2011) 1012–1039, https://doi.org/10.1016/j.jfluchem.2011.06.025.
[16] M.S. Pudovkin, S.V. Kuznetsov, V.Y. Proydakova, V.V. Voronov, V.V. Semashko, Luminescent thermometry based on Ba4Y3F17: Pr3+ and Ba4Y3F17: Pr3+, Yb3+ nanoparticles, Ceram. Int. 46 (8) (2020) 11658–11666, https://doi.org/10.1016/j.ceramint.2020.01.196.
[17] P.P. Fedorov, Systems of alkali and rare-earth metal fluorides, Russ. J. Inorg. Chem. 44 (11) (1999) 1703–1727.
[18] K. Deng, X. Wei, X. Wang, Y. Chen, M. Yin, Near-infrared quantum cutting via resonant energy transfer from Pr3+ to Yb3+ in LaF3, Appl. Phys. B 102 (3) (2011) 555–558, https://doi.org/10.1007/s00340-011-4413-7.
[19] O.A. Morozov, S.L. Korableva, M.S. Pudovkin, A.A. Shakirov, A.A. Shavelev, M. A. Cherosov, A.E. Klimovitskii, Pr3+: LiGdF4 microparticles for optical temperature sensing, Solid State Commun. 351 (2022), 114792, https://doi.org/10.1016/j.ssc.2022.114792.
[20] R.S. Yadav, R.K. Verma, A. Bahadur, S.B. Rai, Structural characterizations and intense green upconversion emission in Yb3+, Pr3+ co-doped Y2O3 nanophosphor, Spectrochim. Acta Mol. Biomol. Spectrosc. 137 (2015) 357–362, https://doi.org/10.1016/j.saa.2014.08.078.
[21] J. He, F. Wei, H. Liu, J. Xia, R. Yang, Y. Lü, Tunable continuous-wave dual-wavelength laser operation of Pr3+: LiYF4 around 900 nm, Laser Phys. Lett. 18 (8) (2021), 085003, https://doi.org/10.1088/1612-202X/ac0fea.
[22] M.R.M. de Sousa, T.O. Sales, W.Q. Santos, W.F. Silva, C. Jacinto, Near-infrared quantum cutting in Pr3+/Yb3+ NaYF4 nanocrystals for luminescent solar converter, J. Lumin. 233 (2021), 117919, https://doi.org/10.1016/j.jlumin.2021.117919.
[23] M.R.M. de Sousa, T.O. Sales, W.Q. Santos, W.F. Silva, C. Jacinto, Near-infrared quantum cutting in Pr3+/Yb3+ NaYF4 nanocrystals for luminescent solar converter, J. Lumin. 233 (2021), 117919, https://doi.org/10.1039/c8nr08348g.
[24] L. Aarts, B.V.D. Ende, M.F. Reid, A. Meijerink, Downconversion for solar cells in YF3: Pr3+, Yb3+, Spectrosc. Lett. 43 (5) (2010) 373–381, https://doi.org/10.1080/00387010.2010.486731.
[25] S. Zhou, G. Jiang, X. Wei, C. Duan, Y. Chen, M. Yin, Pr3+-Doped β-NaYF4 for temperature sensing with fluorescence intensity ratio technique, J. Nanosci. Nanotechnol. 14 (5) (2014) 3739–3742, https://doi.org/10.1166/jnn.2014.8010.
[26] Y. Yang, P. Li, Z. Zhang, Z. Wang, H. Suo, L. Li, Pr3+-based single-band optical ratiometric thermometry, Ceram. Int. 48 (20) (2022) 29907–29912.
[27] C.D. Brites, K. Fiaczyk, J.F. Ramalho, M. Sójka, L.D. Carlos, E. Zych, Widening the temperature range of luminescent thermometers through the intra-and interconfigurational transitions of Pr3+, Adv. Opt. Mater. 6 (10) (2018), 1701318 https://doi.org/10.1002/adom.201701318.
[28] H. Lu, H. Hao, Y. Gao, D. Li, G. Shi, Y. Song, X. Zhang, Optical sensing of temperature based on non-thermally coupled levels and upconverted white light emission of a Gd2 (WO4) 3 phosphor co-doped with in Ho (III), Tm (III), and Yb

(III), Microchim. Acta 184 (2) (2017) 641–646, https://doi.org/10.1007/s00604-016-2070-6.
[29] A. Bednarkiewicz, M. Stefanski, R. Tomala, D. Hreniak, W. Strek, Near infrared absorbing near infrared emitting highly-sensitive luminescent nanothermometer based on Nd 3+ to Yb 3+ energy transfer, Phys. Chem. Chem. Phys. 17 (37) (2015) 24315–24321, https://doi.org/10.1039/c5cp03861h.
[30] H.U. Fangfang, Z.H.A.O. Zhangmei, C.H.I. Fengfeng, W. Xiantao, Y.I.N. Min, Structural characterization and temperature-dependent luminescence of CaF2: Tb3+/Eu3+ glass ceramics, J. Rare Earths 35 (6) (2017) 536–541, https://doi.org/10.1016/S1002-0721(17)60945-1.
[31] L. Fu, Z. Fu, Y. Yu, Z. Wu, J.H. Jeong, An Eu/Tb-codoped inorganic apatite Ca5 (PO4) 3F luminescent thermometer, Ceram. Int. 41 (5) (2015) 7010–7016, https://doi.org/10.1016/j.ceramint.2015.02.004.
[32] J. Liu, R. Van Deun, A.M. Kaczmarek, Eu3+, Tb3+-and Er3+, Yb3+-doped α-MoO3 nanosheets for optical luminescent thermometry, Nanomaterials 9 (4) (2019) 646, https://doi.org/10.3390/nano9040646.
[33] A. Zhou, F. Song, F. Song, M. Feng, K. Adnan, D. Ju, X. Wang, Optical thermometry using fluorescence intensities multi-ratios in NaGdTiO4: Yb3+/Tm3+ phosphors, Opt. Mater. 78 (2018) 438–444, https://doi.org/10.1016/j.optmat.2018.02.047.
[34] M.S. Pudovkin, D.A. Koryakovtseva, E.V. Lukinova, S.L. Korableva, R. S. Khusnutdinova, A.G. Kiiamov, V.V. Semashko, Luminescence nanothermometry based on Pr3+: LaF3 single core and Pr3+: LaF3/LaF3 core/shell nanoparticles, 2019, Adv. Mater. Sci. Eng. (2019), https://doi.org/10.1155/2019/2618307.